



1 **AIMERG: a new Asian precipitation dataset (0.1°/half-hourly, 2000-2015) by calibrating GPM**
2 **IMERG at daily scale using APHRODITE**

3 Ziqiang Ma¹, Jintao Xu², Siyu Zhu¹, Guoqiang Tang^{3,4}, Yuanjian Yang⁵, Zhou Shi², Yang Hong^{1,6}

4 ¹*Institute of Remote Sensing and Geographical Information Systems, School of Earth and Space Sciences, Peking*
5 *University, Beijing, 100871, China*

6 ²*Institute of Agricultural Remote Sensing and Information Technology Application, College of Environmental and*
7 *Resource Sciences, Zhejiang University, Hangzhou, 310058, China*

8 ³*University of Saskatchewan Coldwater Lab, Canmore, Alberta, Canada, T1W 3G1*

9 ⁴*Centre for Hydrology, University of Saskatchewan, Saskatoon, Saskatchewan, Canada, S7N 1K2*

10 ⁵*School of Atmospheric Physics, Nanjing University of Information Science and Technology, Nanjing 210044, China*

11 ⁶*School of Civil Engineering and Environmental Science, University of Oklahoma, Norman, OK, 73019, United States*

12 Correspondences: Ziqiang Ma (ziqma@pku.edu.cn); Prof. Yang Hong (yanghong@ou.edu)

13



14 **AIMERG: a new Asian precipitation dataset (0.1°/half-hourly, 2000-2015) by calibrating GPM**
15 **IMERG at daily scale using APHRODITE**

16

17 **Highlights**

- 18 ● **A new effective daily calibration approach, DSTDCA, for improving GPM IMERG**
- 19 ● **A new AIMERG precipitation data (0.1°/half-hourly, 2000-2015, Asia) was provided**
- 20 ● **Bias of AIMERG was significantly improved compared with that of IMERG**
- 21 ● **APHRODITE is more suitable than GPCC in anchoring IMERG over the Asia**

22

23

24

25

26

27

28



29 **Abstract**

30 Precipitation estimates with finer quality and spatio-temporal resolutions play significant roles in
31 understanding the global and regional cycles of water, carbon and energy. Satellite-based precipitation
32 products are capable of detecting spatial patterns and temporal variations of precipitation at finer
33 resolutions, which is particularly useful over poorly gauged regions. However, satellite-based
34 precipitation product are the indirect estimates of precipitation, inherently containing regional and
35 seasonal systematic biases and random errors. In this study, focusing on the potential drawbacks in
36 generating Integrated Multi-satellitE Retrievals for Global Precipitation Measurement (IMERG) and its
37 recently updated retrospective IMERG in Tropical Rainfall Measuring Mission (TRMM) era (finished in
38 July, 2019), which were only calibrated at monthly scale using ground observations, Global Precipitation
39 Climatology Centre (GPCC, 1.0°/Monthly), we aimed to propose a new calibration algorithm for IMERG
40 at daily scale, and to provide a new AIMERG precipitation dataset (0.1°/ half-hourly, 2000-2015, Asia)
41 with better quality, calibrated by Asian Precipitation Highly Resolved Observational Data Integration
42 (APHRODITE, 0.25°/Daily) at daily scale for the Asian applications. And the main conclusions included
43 but not limited to: (1) the proposed daily calibration algorithm (Daily Spatio-Temporal Disaggregation
44 Calibration Algorithm, DSTDCA) was effective in considering the advantages from both satellite-based
45 precipitation estimates and the ground observations; (2) AIMERG performed better than IMERG at
46 different spatio-temporal scales, in terms of both systematic biases and random errors, over the China
47 Main land; and (3) APHRODITE demonstrated significant advantages than GPCC in calibrating the



48 IMERG, especially over the mountainous regions with complex terrain, e.g., the Tibetan Plateau.
49 Additionally, Results of this study suggests that it is a promising and applicable daily calibration
50 algorithm for GPM in generating the future IMERG in either operational scheme or retrospective manner.

51 The AIMERG data record (0.1°/half-hourly, 2000-2015, Asia) is freely available at <http://argi->
52 basic.hihanlin.com:8000/d/d925fecf60/. Additionally, the AIMERG data is also freely accessible at
53 <https://doi.org/10.5281/zenodo.3609352> (for the period from 2000 to 2008) (Ma et al., 2020a) and
54 <http://doi.org/10.5281/zenodo.3609507> (for the period from 2009 to 2015) (Ma et al., 2020b).

55 **Keywords: Precipitation; IMERG; APHRODITE; Calibration; Daily scale; Asia;**

56

57 **1. Introduction**

58 Precipitation is among the most essential hydroclimatic factors, and also most difficult to estimate
59 due to its great small-scale variabilities (Yatagai et al., 2012; Huffman et al., 2019). High spatio-temporal
60 resolution precipitation dataset with fine quality is essential for various scientific and operational
61 applications, including but not limited to driving the hydrological models, and supporting the predictions
62 of droughts and floods (Beck et al., 2017, 2018). There are mainly two principal approaches for
63 measuring the global precipitation: ground-based gauge observing, and satellite-based remote sensing,
64 which resulting in three mainstreams of global precipitation products, namely gauge analysis



65 precipitation data, satellite-based only precipitation estimates, and satellite-gauge combined
66 precipitation products, based on the consideration that ground-based gauge data are clearly important
67 for anchoring the satellite estimates (Huffman et al., 2007, 2014, 2019).

68 In recent years, a large number of quasi-global satellite precipitation products with various
69 temporal and spatial resolutions have been developed and released to the public, such as the PMW-based
70 CPC Morphing technique (CMORPH) (hereafter, for Acronyms, see the Appendix) (Joyce et al., 2004),
71 and IR-based PERSIANN (Sorooshian et al., 2000) and PERSIANN-CCS (Hong et al., 2004). As the
72 milestone in the satellite-based precipitation measurement process, the TRMM and its successor GPM
73 developed a flexible framework for generating the most popular near-real-time precipitation products,
74 TMPA (1998-present, $0.25^{\circ}/3$ hourly) and IMERG (2014-present, $0.1^{\circ}/$ half-hourly), as well as the
75 retrospective IMERG (2000-present, $0.1^{\circ}/$ half-hourly) from GPM era to TRMM era, which aimed at
76 intercalibrating, merging, and interpolating all MW estimates of the GPM constellation, IR estimates,
77 gauge observations, and other data from potential sensors at $0.1^{\circ} \times 0.1^{\circ}$ and half-hourly temporal
78 resolutions (Huffman et al., 2014, 2019). The “Final” version of IMERG (Hereafter refer to IMERG),
79 incorporated the monthly gauge analysis, provides the state-of-the-art precipitation estimate with finest
80 spatio-temporal resolutions so far, while it still greatly overestimates the precipitation at daily and hourly
81 scales from regions to regions, especially over the mountainous areas, such as the Tibetan Plateau, China
82 (Tang et al., 2016; Lu et al., 2019; Xu et al., 2019), which is greatly potentially resulted by the calibration
83 procedures in the process of generating the IMERG. Currently, the IMERG product (following the



84 TMPA approach) (Huffman et al., 2007) has been produced by anchoring the satellite-based only
85 precipitation estimates using the monthly analysis Satellite-Gauge product (2.5°/monthly, 1979 to the
86 present, delayed by about 3 months) from the GPCP (Adler et al., 2003, 2018), therefore, the IMERG
87 performed better at monthly and annual scale than those at finer temporal scales (e.g., daily, hourly). And
88 how to calibrate the IMERG at daily scale is one of the next vital focuses by the GPM.

89 Satellite-based precipitation products have significant advantages in detecting the variations of
90 precipitation at finer spatio-temporal resolutions, especially over the poorly gauged regions. However,
91 as the indirect estimates of precipitation, satellite-based precipitation products are inherently containing
92 regional and seasonal systematic biases and random errors (Ebert et al., 2007; Shen et al., 2014), which
93 could be effectively alleviated by anchoring the satellite-based only precipitation products using gauge-
94 based observations (Huffman et al., 2007; Xie and Xiong, 2011), and great efforts have been focused on
95 generating the Satellite-Gauge combined precipitation products with finer accuracies, most of which
96 calibrations on satellite-based precipitation were conducted at the monthly scale, and very limited
97 explorations at the daily scale (Adler et al., 2003; Huffman et al., 2007, 2014, 2019).

98 As for anchoring the satellite precipitation estimates, the quality and spatio-temporal resolutions
99 of the gauge analysis precipitation data are the key factors. Though the GPCP has developed a series of
100 gauge-based precipitation analysis datasets with the quality and spatio-temporal resolutions continually
101 improved, accurate estimations of precipitation over the land is still greatly difficult over the land with



102 limited networks of rain gauges. In Asia, great efforts also have been mainly paid on generating gauge-
103 analysis precipitation products at the monthly scale (Chen et al., 2002; Mitchell and Jones 2005;
104 Matsuura and Willmott 2009; Schneider et al. 2008), and limited explorations at the daily scale, e.g.,
105 Rajeevan and Bhate (2009) explored daily grid precipitation data over India with data from more than
106 2,500 rain gauges. Meanwhile, significant differences among those products had been reported by
107 Yatagai et al (2005, 2012). To more accurately monitor and predict the Asian hydro-meteorological
108 environment, the APHRODITE project (starting in 2006) aimed at developing the state-of-the-art
109 gridded precipitation datasets at the resolutions of 0.25° /daily covering the entire Asia based on the
110 largest numbers of ground observations from multi-sources. Since the release of APHRODITE products
111 (1951-2015, 0.25° /daily, Last update October 5, 2018), APHRODITE daily grid precipitation data sets
112 have been widely used, and it distinguished from other gauge analysis data by considering the different
113 interpolation schemes and climatology characteristics, especially over the mountainous regions with
114 complex terrain, e.g., the Tibetan Plateau (Yatagai et al., 2012).

115 The aim of this study is to explore the calibration approach at daily scale on the retrospective
116 IMERG data using APHRODITE product, in both TRMM and GPM era, from 2000 to 2015. Meanwhile,
117 a new calibration approach, Daily Spatio-Temporal Disaggregation Calibration Algorithm (DSTDCA),
118 was proposed and suggested for the GPM in their future algorithms; and a new AIMERG precipitation
119 dataset (0.1° / half-hourly, 2000-2015, Asia) (Ma et al., 2020a, b) with better quality was to be provided
120 publicly for the Asian applications.



121

122 **2. Data**

123 **2.1 IMERG**

124 To generate the IMERG product, GPM focused on intercalibrating, merging, and interpolating “all”
125 satellite MW-based precipitation estimates, together with MW-calibrated IR-based precipitation
126 estimates, precipitation gauge analyses, and potentially other precipitation estimators at fine spatio-
127 temporal scales for the both TRMM and GPM eras over the entire globe. Currently, IMERG is at its
128 Version 06 stage (https://pmm.nasa.gov/sites/default/files/document_files/IMERG_ATBD_V06.pdf),
129 based on which the TRMM era IMERG has been completed at the end of September, 2019, and IMERG
130 is now available back to June 2000 (half-hourly/0.1°) ([https://pmm.nasa.gov/data-
131 access/downloads/gpm](https://pmm.nasa.gov/data-access/downloads/gpm)). IMERG “Final” run combines the GPCC Monitoring product, the V8 Full Data
132 Analysis for the majority of the time (currently 1998-2016), and the V6 Monitoring Product from 2017
133 to the then-present. The Monitoring Product is poster about two months after the month of observation
134 from ~7,000-8,000 stations world-wide (Schneider et al. 2014, 2018).

135 **2.2 APHRODITE**

136 Since the release APHRODITE product (0.25°/Daily, 1951-2007), it has been widely used as one of
137 state-of-the-art daily grid precipitation datasets over the Asia, for hydro-climatological related studies



138 (Yatagai et al., 2012). APHRODITE has been demonstrated to replicate ‘ground truth’ observations very
139 well (Duncan and Bigg, 2012) and represents the best tool for analyzing historical precipitation variability
140 and change. Recently, the APHRODITE data had been updated from the former period 1951-2007 to a
141 longer period 1951-2015, in September, 2018, with continuous efforts of quality control (QC) flagging
142 some data (Hamada et al., 2011). The APHRODITE data could be available through the website
143 (<http://aphrodite.st.hirosaki-u.ac.jp/download/>).

144 **2.3 CMPA**

145 The China Merged Precipitation Analysis (CMPA, 0.1°/hourly, 2008-2015) were generated by using
146 hourly rain gauge data at more than 30, 000 automatic weather stations in China, with the combination of
147 the CMORPH precipitation product, and provided by the Chinese Meteorological Administration
148 (<http://data.cma.cn>) (Shen et al., 2010). The inverse distance weighting (IDW) interpolation method was
149 adopted to estimate the areal precipitation distribution based on the gauge observations (Yong et al., 2010),
150 but uncertainty still existed in the interpolated precipitation field particularly over West China with
151 relatively sparse gauge networks. For grid boxes with gauges, the observed precipitation values are
152 exactly the gauge observation or the averaged observation when more than one gauge locates in a grid.

153 **2.4 Point-based rain gauge data from meteorological stations**

154 The hourly rain gauge datasets from 57, 835 national ground stations used in this study, in 2015,
155 were collected from the National Meteorological Information Center of CMA (<http://data.cma.cn>). All



156 the gauge data have undergone strict quality control in three levels, which includes (1) the extreme values'
157 check, (2) internal consistency check, and (3) spatial consistency check (Shen et al., 2010). Most gauges
158 are located over the eastern and southern parts of the Mainland China, and relatively sparse gauge network
159 are located across the northern and western parts, especially over the Tibetan Plateau. The limited number
160 of gauges could be a source of error in evaluation of satellite precipitation products in such areas (Shen
161 et al., 2014).

162 **2.5 Point-based rain gauge data from hydrological stations**

163 The hourly ground precipitation observations from around 500 hydrological stations (the number of
164 station varied from year to year) used in this study were collected from Hydrology Bureau of Zhejiang
165 Province, southeastern China (<http://data.cma.cn/>). The quality control follows two steps: (1) the datasets
166 are filtered by threshold value after being collected from rain gauges; (2) the outliers are identified through
167 manual processing. With careful data quality control, the rain gauge datasets have satisfying performances
168 on the accuracy and validity.

169 There were five datasets used in this study (refer to Table 1 for a summary of the datasets). IMERG
170 and APHRODITE were used for generating the AIMERG data, and the others were used for evaluating
171 and comparing the IMERG and AIMERG at different scales.

172



173 **Table 1.** List of satellite-based, gauge-based, and satellite-gauge combination precipitation products used
 174 in this study.

Short name	Full name	Spatial and temporal sampling	Time period	References
	Integrated Multi-satellitE			Huffman et al. (2019)
IMERG	Retrievals for Global Precipitation Measurement	0.1°/half-hourly	2000-present	https://pmm.nasa.gov/data-access/downloads/gpm (last access: 17 January 2020)
	Asian Precipitation Highly Resolved Observational			Yatagai et al. (2012)
APHRODITE	Data Integration Towards Evaluation of Water Resources	0.25°/daily	1951-2015	http://aphrodite.st.hirosaki-u.ac.jp/download/ (last access: 17 January 2020)
	China Merged Precipitation Analysis			Shen et al. (2014)
CMPA		0.1°/hourly	2008-present	http://data.cma.cn (last access: 17 January 2020)
	Point-based rain gauge data	hourly	2010-present	Shen et al. (2010) http://data.cma.cn (last access: 17 January 2020)

175

176

177

178 **3. Methodology**



179 **3.1 Calibration Procedure of the Daily Spatio-Temporal Disaggregation Calibration**

180 **Algorithm, DSTDCA**

181 According to previous evaluation investigations on IMERG (Lu et al., 2019; Xu et al., 2019), there
182 were at least two characteristics resulting its significant overestimations: (1) the amplitude of hourly or
183 half-hourly estimated rainfall rates were significantly amplified by IMERG compared with ground
184 observations, which might be caused by the benchmark of GPCC and GPCP SG data for calibrations, and
185 (2) the IMERG algorithm is generally over detecting precipitation events, resulting a large fraction of
186 false alarm but unreal precipitation events. Therefore, this study selected the APHRODITE data as the
187 benchmark for calibrating IMERG at daily scale, based on the proposed approach, DSTDCA, and the
188 main steps of the DSTDCA were shown as follows:

189 (1) IMERG data (0.1° /half-hourly) were accumulated to those (0.1° /daily), which were used to
190 generate the spatial disaggregation weights. As the spatial resolution of APHRODITE data was 0.25° , the
191 moving window size of 3 by 3 was selected, and the daily spatial disaggregation weights (0.1°) based on
192 IMERG was obtained by calculating the ratios between the daily rainfall accumulations at the central grid
193 and the average daily rainfall accumulations in the corresponding 3×3 window. The daily spatial
194 disaggregation weights considered the relative spatial patterns of the precipitation captured by the IMERG;

195 (2) Based on the daily precipitation accumulations of IMERG, the half-hourly temporal
196 disaggregation weights (0.1°) was derived by calculating the ratios between the each half-hourly



197 precipitation estimates and the corresponding daily precipitation estimates. If the daily accumulation
198 estimate is equal to zero, then each half-hourly temporal disaggregation weights were all set as zero;

199 (3) As there were a small fraction of grids in APHRODITE with no data at daily scale, the no data
200 grids in APHRODITE data were firstly filled with the data according to its nearest neighbor with effective
201 value;

202 (4) Spatial calibrations: the daily calibrated IMERG using APHRODITE data were obtained by
203 multiplying the spatial disaggregation weights based on IMERG ($0.1^\circ/\text{daily}$) from step (1) by daily
204 APHRODITE data ($0.25^\circ/\text{daily}$) from step (3);

205 (5) Temporal calibrations: the half-hourly calibrated IMERG were obtained by multiplying the half-
206 hourly temporal disaggregation weights ($0.1^\circ/\text{half-hourly}$) from step (2) by the daily calibrated IMERG
207 from step (3);

208 (6) By considering the situations that APHRODITE data captured the precipitation while the IMERG
209 did not, the half-hourly calibrated IMERG were further processed by equally disaggregating the value
210 from the daily APHRODITE data at the corresponding grid into 48 half-hourly periods, which were
211 regarded as the half-hourly calibrated IMERG values in the corresponding day;



212 (7) By considering the situations that IMERG data captured the precipitation while the APHRODITE
213 did not, the 48 half-hourly calibrated IMERG values in corresponding days and locations were set as zero,
214 to meet the ground truth observations;

215 After all the above-mentioned procedures, the Final calibrated AIMERG (0.1°/ half-hourly) data
216 were obtained by considering the both the total precipitation controls and the effective precipitation events
217 measured by the “ground truth” observations by APHRODITE data over the Asia.

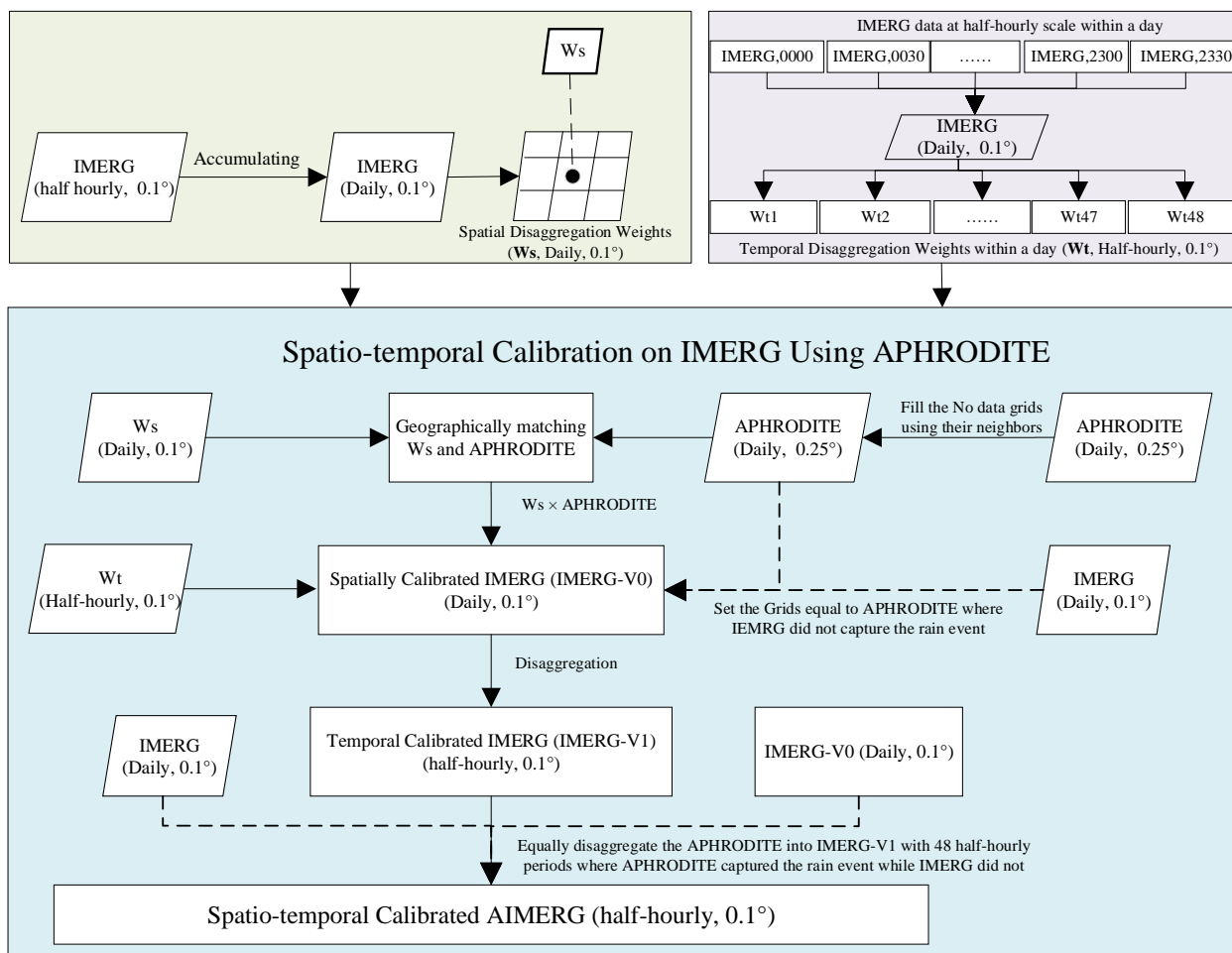


Figure 1. The flowchart of the Daily Spatio-Temporal Disaggregation Calibration Algorithm, DSTDCA, to generate the AIMERG dataset over the Asia, 2000-2015

3.2 Evaluation Metrics

To evaluate the IMERG and its calibrations comprehensively, seven metrics (CC, MAE, BIAS, RMSE, POD, FAR, CSI) were selected (Tang et al., 2016). Generally, CC is used to describe the



224 agreements between satellite estimates and gauge observations; MAE, RMSE, and BIAS are used to
 225 indicate the error and bias of satellite estimates compared with gauge observations; and the POD, FAR,
 226 and CSI are used to demonstrate the capabilities to correctly capture the precipitation events of satellite
 227 precipitation estimates against the ground observations. The detailed information of these evaluation
 228 metrics are listed in Table 2.

229 **Table 2** Formulas and perfect values of the evaluation metrics used in this study^a.

Statistic metrics	Equation	Perfect value
Correlation Coefficient (CC)	$CC = \frac{\frac{1}{N} \sum_{n=1}^N (S_n - \bar{s})(G_n - \bar{G})}{\sigma_S \sigma_G}$	1
Mean Error (ME)	$ME = \sum_{n=1}^N (S_n - G_n)$	0
Relative Bias (BIAS)	$BIAS = \frac{\sum_{n=1}^N (S_n - G_n)}{\sum_{i=1}^n G_n} \times 100\%$	0
Root Mean Square Error (RMSE)	$RMSE = \sqrt{\frac{1}{N} \sum_{n=1}^N (S_n - G_n)^2}$	0
Probability of Detection (POD)	$POD = \frac{n_{11}}{n_{11} + n_{01}}$	1
False Alarm Ratio (FAR)	$FAR = \frac{n_{10}}{n_{11} + n_{10}}$	0
Critical Success Index (CSI)	$CSI = \frac{n_{11}}{n_{11} + n_{10} + n_{01}}$	1

230 ^aNotation: n is the sample numbers; S_n is satellite precipitation estimate; G_n is gauge-based precipitation; σ_G is the standard deviations of
 231 gauge-based precipitation; σ_S is the standard deviations of satellite-based precipitation estimate. n₁₁ is the precipitation event detected by
 232 both gauge and satellite simultaneously; n₁₀ is the precipitation event detected by the satellite but not detected by the gauge; n₀₁ is contrary
 233 to n₁₀; n₀₀ is the precipitation events detected neither by the gauge nor the satellite.

234

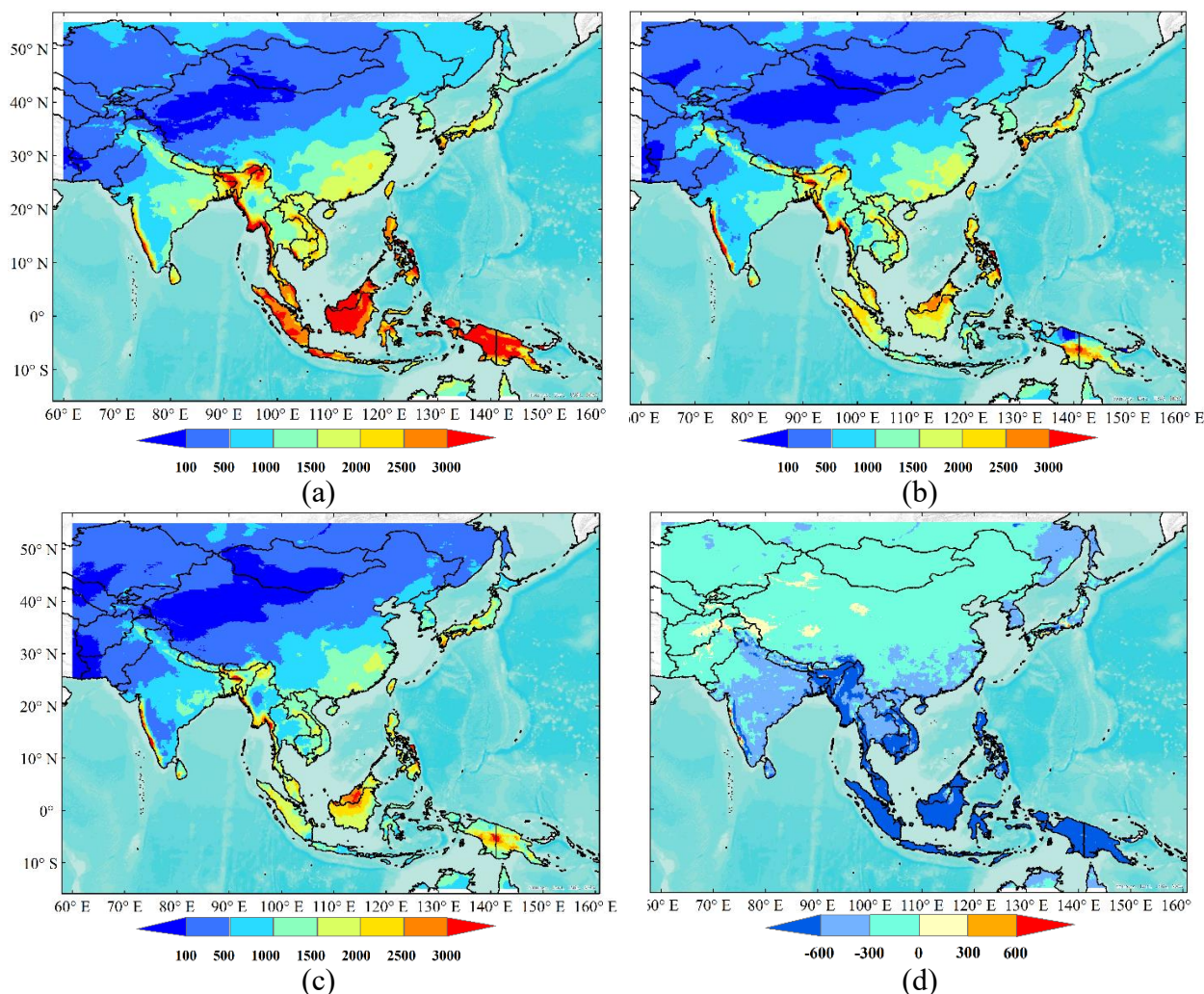


235 **4. Results**

236 **4.1 AIMERG Product**

237 Generally, both IMERG and APHRODITE shared similar spatial patterns with precipitation volumes
238 decreasing from southeast to northwester in Asia, while compared with APHRODITE data (Fig. 2b),
239 IMERG greatly overestimated the precipitation over Arunachal Pradesh, coastal Indochina and Western
240 Ghats, and the Indonesia (Fig. 2a). Corrected by APHRODITE, the spatial patterns and volumes of
241 AIMERG were much more similar to those of APHRODITE, especially along the Himalayas, coastal
242 Indochina and Western Ghats, and the Indonesia (Fig. 2c). Compared with APHRODITE, AIMERG
243 seems floating up and down in terms of the volumes, for instance, AIMERG is larger and smaller than
244 APHRODITE in eastern Indonesia and northeastern Asia, respectively. Though AIMERG are smaller
245 than IMERG over most regions, there are still some areas where the volumes of AIMERG are larger than
246 those of IMERG, e.g., in western Tibetan Plateau, Middle East, and along the western coast of India (Fig.
247 2d).

248

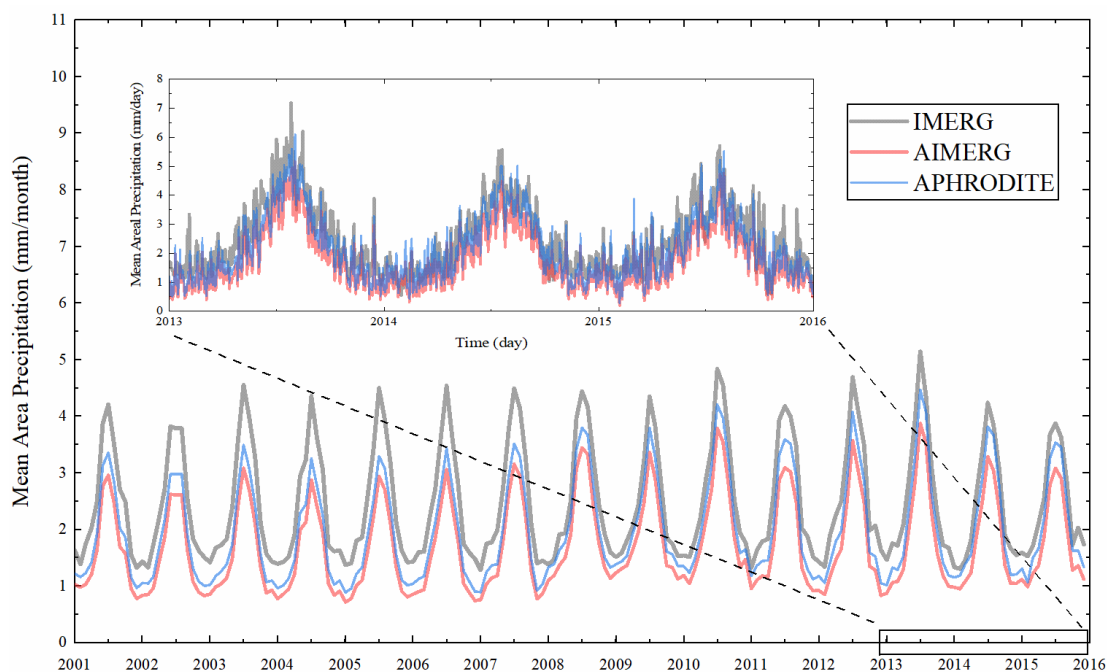


249 Figure 2. Spatial patterns of Asian mean annual gridded precipitation products of (a) IMERG, 0.1°, (b)
250 APHRODITE, 0.25°, and (c) AIMERG, 0.1°, and (d) AIMERG-IMERG, 0.1°, respectively, during the
251 period of 2001-2015. The background map used in this study was provided by Esri, USGS and NOAA
252 (http://goto.arcgisonline.com/maps/World_Terrain_Base, last access: 17 January 2020).

253



254 The temporal patterns of the mean areal precipitation over the Monsoon Asia of the three products
255 demonstrated that the systematic bias of IMERG was significantly reduced in both dry and wet seasons,
256 shown in Fig. 3. IMERG is around 1.5 times larger than APHRODITE at monthly scale. Though much
257 more close to the APHRODITE, AIMERG is still a little smaller than the APHRODITE, which means
258 the calibration algorithm proposed by this study tends to underestimate the precipitation compared with
259 calibration benchmark, APHRODITE. At daily scale, IMERG are generally larger than APHRODITE,
260 while at some special days, APHRODITE are larger than IMERG, which might result the AIMERG may
261 be also larger than IMERG.



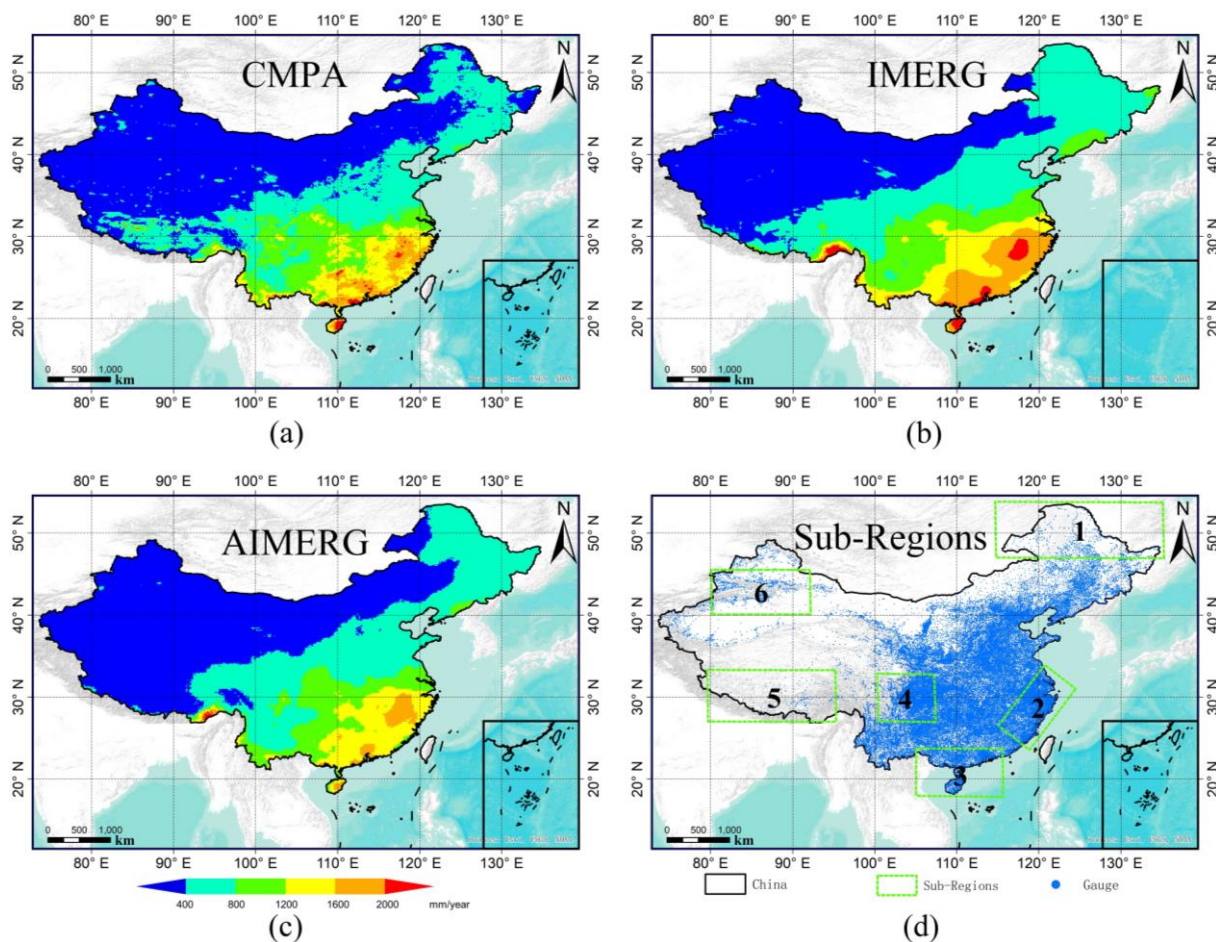
262



263 Figure 3. The temporal variations of mean Asian gridded precipitation products of IMERG, APHRODITE,
264 and AIMERG, respectively, during the period of 2001-2015.

265 **4.2 Assessments on IMERG and AIMERG at national and regional scales**

266 The spatial patterns of CMPA demonstrated much more similar to those of AIMERG, especially
267 in the southeastern China where dense rain gauges are located, while both CMPA and IMERG
268 overestimated the precipitation along the Himalayas where the meteorological gauges were sparse and
269 mainly the satellite-based observations were applied (Fig. 4). Obviously, the IMERG significantly
270 overestimated the precipitation in the southeast coast of China, where typhoons always visit (Fig. 4 b).



271

272 Fig.4 Spatial patterns of (a) CMPA, (b) IMERG, and (c) AIMERG over China Mainland From 2008~2015,

273 and (d) the spatial distributions of the ~ 50, 000 automatic meteorological stations in China Main land.

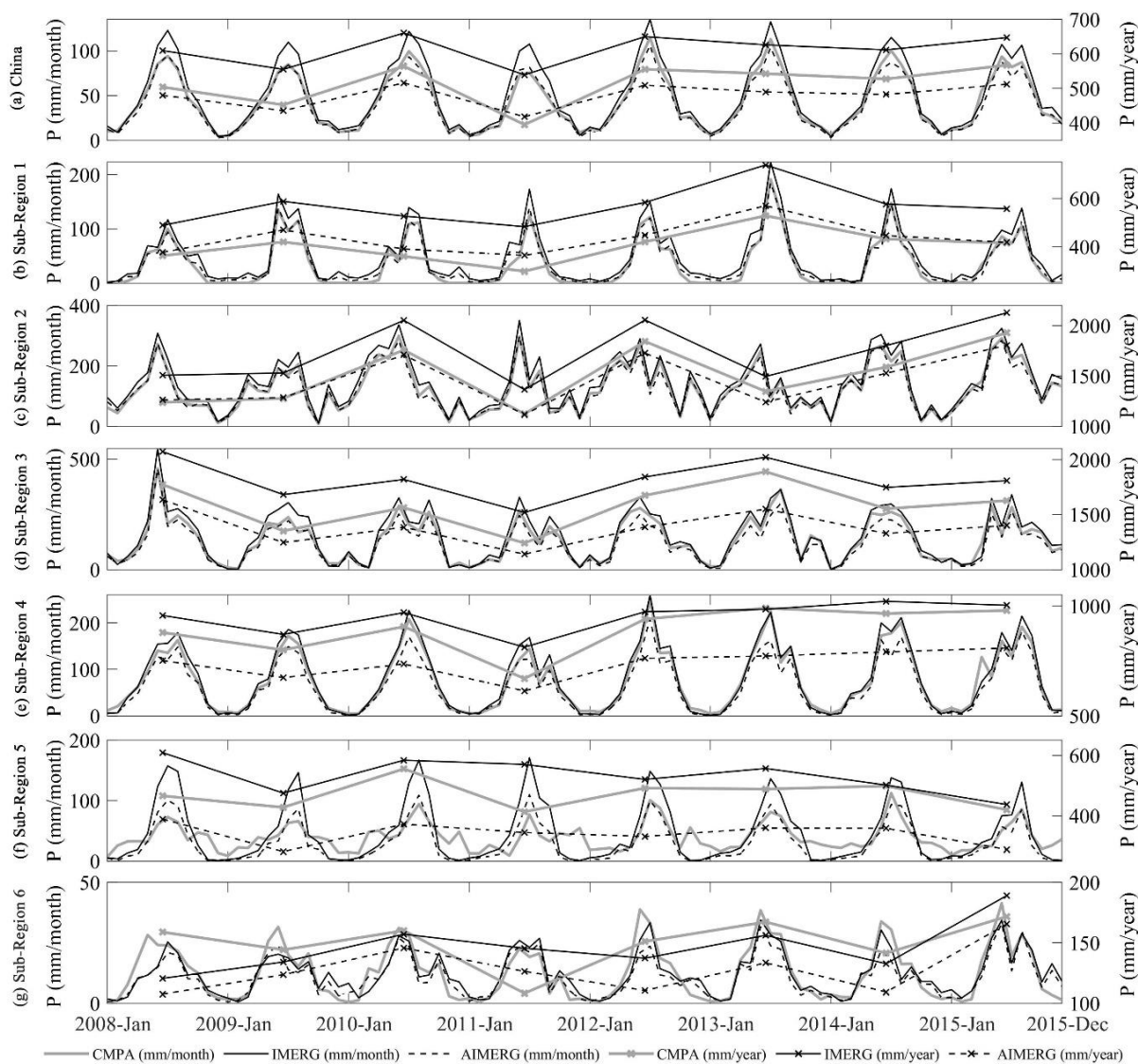
274 The background map used in this study was provided by Esri, USGS and NOAA

275 (http://goto.arcgisonline.com/maps/World_Terrain_Base, last access: 17 January 2020).

276



277 The magnitudes of IMERG, AIMERG, and CMPA were compared at national and regional scale
278 over the China Mainland from 2008 to 2015 (Fig. 5). Generally speaking, CMPA and AIMERG were
279 almost same, and were both significantly smaller than IMERG at both annual and monthly scales,
280 additionally, CMPA was still a little bit larger than AIMERG over the China Mainland, which could be
281 possibly resulted from the use of satellite observations in the CMPA and IMERG (Fig. 6a). The overall
282 situations of the three product in sub-region 1 and 2 were similar with those over the China Mainland
283 (Fig. 6 b-c), while both CMPA and IMERG were both significantly larger than AIMERG (Fig. 6 d-f). In
284 sub-region 6, the Tianshan Mountains, CMPA were almost even larger than IMERG, which indicated that
285 large uncertainties should be focused on (Fig. 6 g).

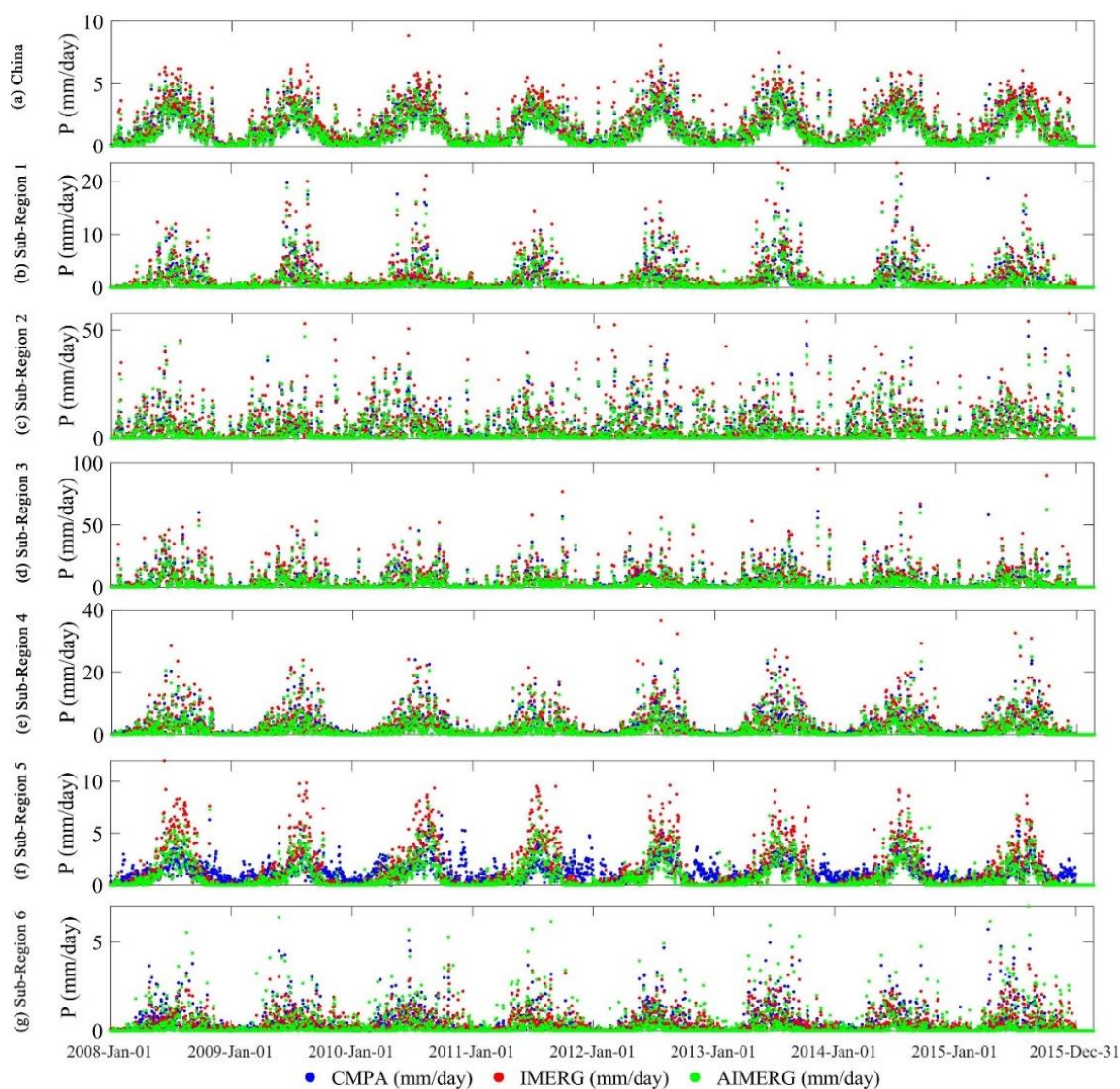


286

287 Fig.5 The temporal patterns of mean areal precipitation of the IMERG, CMPA, and AIMERG, over China
 288 Mainland and sub-regions from 2008 to 2015, at monthly and annual scales.



289 As this study aimed to propose a new algorithm for calibrating the IMERG product at the daily
290 scale, the daily spatial patterns of IMERG, CMPA, and AIMERG were explored, which generally agreed
291 with those of IMERG, CMPA, and AIMERG at monthly scale (Fig. 6). In mountainous region, along the
292 Himalayas, with relatively small precipitation, CPMA were greatly larger and smaller than the other two
293 products (both IMERG and AIMERG) in dry seasons and wet seasons respectively (Fig. 6 f). One
294 phenomenon should be noted that the CPMA seems abnormal along the Himalayas, which might be
295 resulted by the limited ground observations used in CMPA, shown in Fig 4d, while APHRODITE data
296 integrated large numbers of ground observations from the neighbor countries, such as India, Nepal,
297 Bhutan, providing valuable information for retrieving high quality precipitation product around the
298 Tibetan Plateau (Yatagai, 2012). Calibrated by APHRODITE at daily scale, AIMERG were significantly
299 smaller than IMERG and CMPA at both annual and monthly scale, while there were also some situations
300 that AIMERG were larger than IMERG and CMPA at daily scale, for example in sub-region 6, over the
301 Tianshan mountains.



302

303

Fig.6 The temporal patterns of mean areal precipitation of the IMERG, CMPA, and AIMERG, over

304

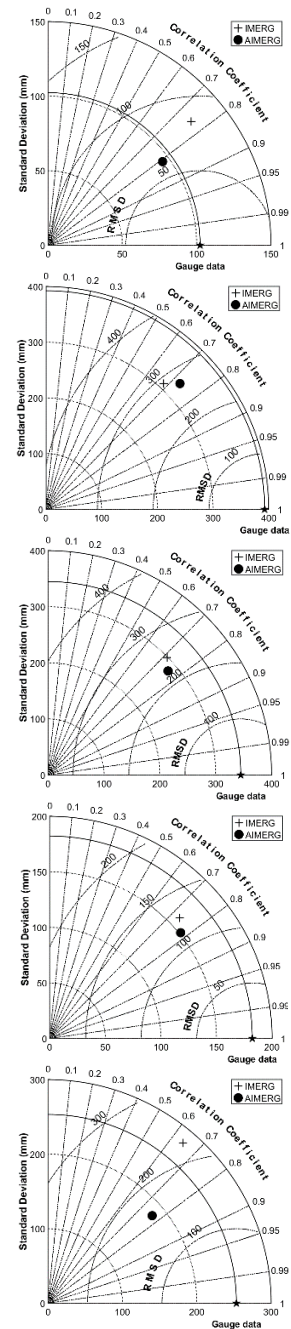
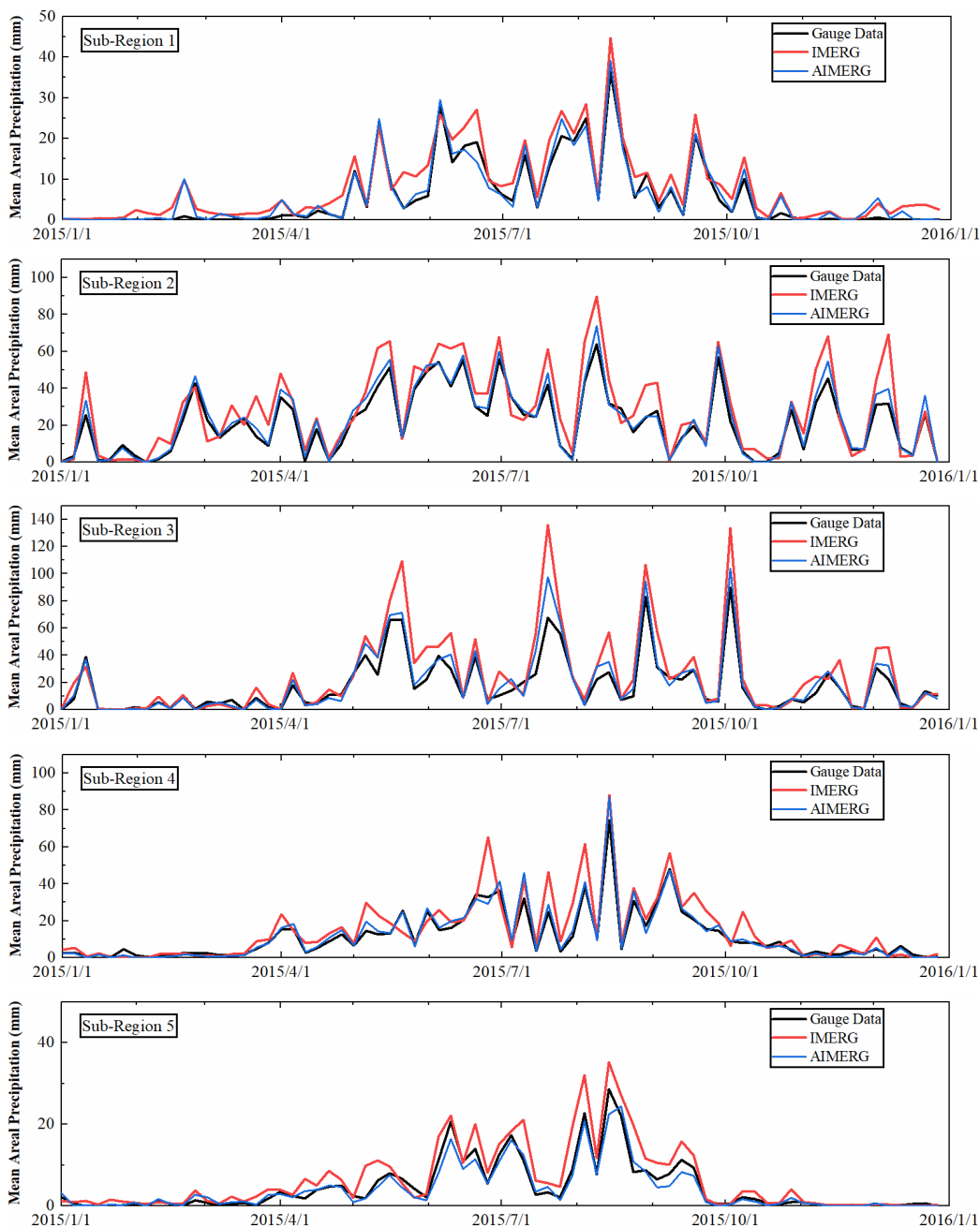
China Mainland and sub-regions from 2008 to 2015, at daily scale.

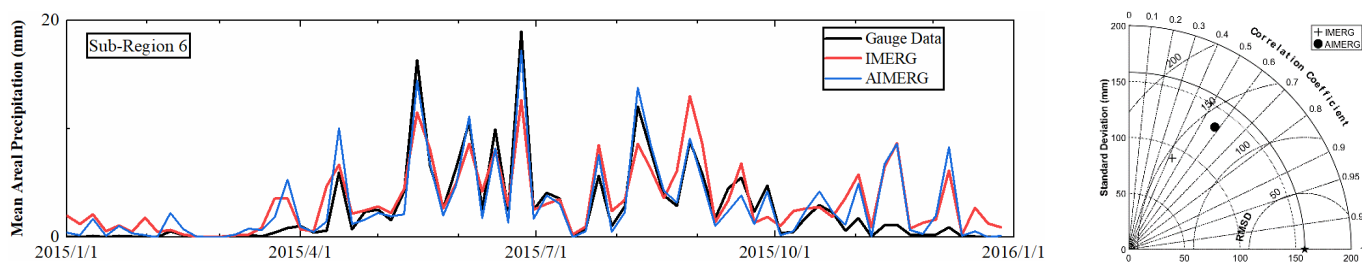
305



306 Hourly ground observation data from more than 50, 000 meteorological stations were used to assess
307 the quality of the IMERG and its calibrations, AIMERG, over the six sub-regions, in 2015 (Fig. 7). The
308 temporal patterns and volumes of mean areal precipitation by AIMERG and ground observations were
309 almost same, while IMERG were generally larger than AIMERG and ground observations. Meanwhile,
310 the IMERG still has the problems in overestimating and underestimating the precipitation in dry seasons
311 (relatively large precipitation occurring) and wet seasons (relatively small precipitation happening),
312 respectively, for example in sub-region 6, over the Tianshan Mountains. In terms of quantitative indices
313 (Standard deviation, RMSD, and CC), AIMERG generally outperformed the IMERG against the ground
314 observations, especially in sub-region 5, along the Himalayas, which indicated that the ground
315 information from the neighbor countries integrated into the APHRODITE data greatly benefited the
316 calibration results, AIMERG.

317

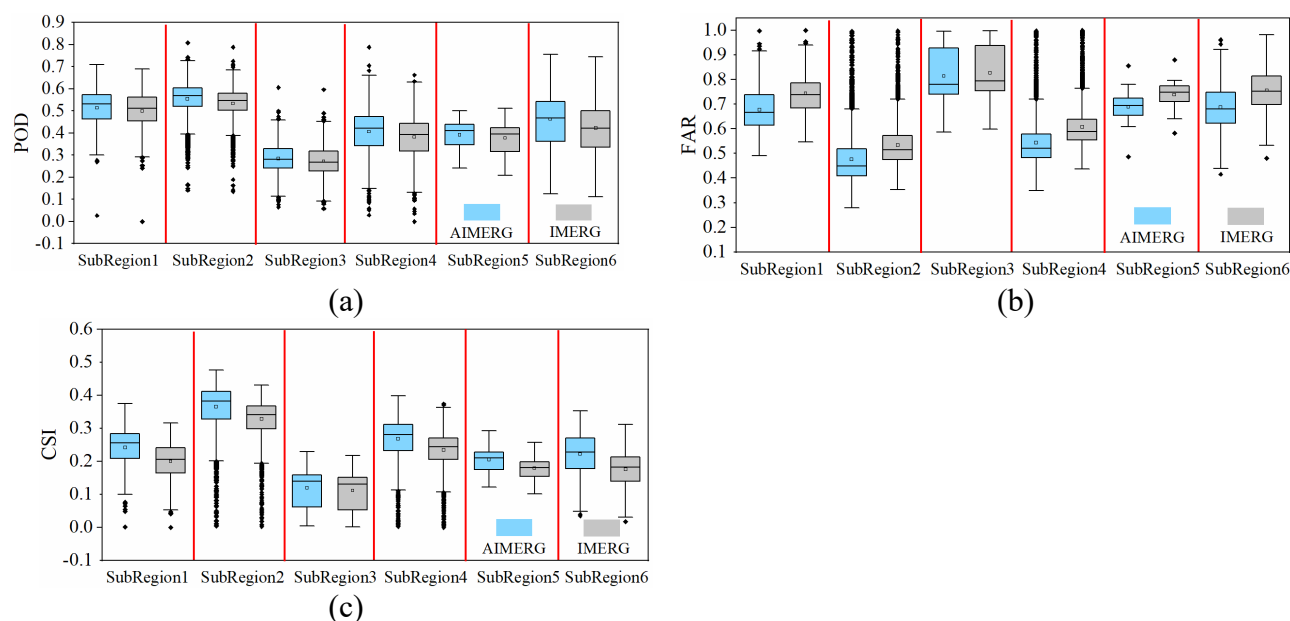




318 Figure 7. The temporal patterns and the volumes of IMERG, ground observations, and AIMERG, in six
319 sub-regions at daily scale; and the Taylor diagrams of performances on IMERG and AIMERG against
320 ground observations in terms of centered root-mean-square difference, correlation coefficient and
321 standard deviation in the six sub-regions at hourly scale, in 2015.

322

323 Figure 8 illustrated the numerical distributions of contingency statistics for IMERG and AIMERG,
324 at hourly scale, in six sub-regions, 2015. Generally, the POD values of AIMERG were larger than those
325 of IMERG (Fig. 8a), and FAR values of AIMERG were overall smaller than those of IMERG in each
326 sub-regions (Fig. 8b), which resulted the better performances of the comprehensive index, CSI,
327 combining both the characteristics of POD and FAR, in each sub-regions (Fig. 8c). Additionally, both the
328 IMERG and AIMERG performed best in sub-region 2, and worst in sub-region 3.



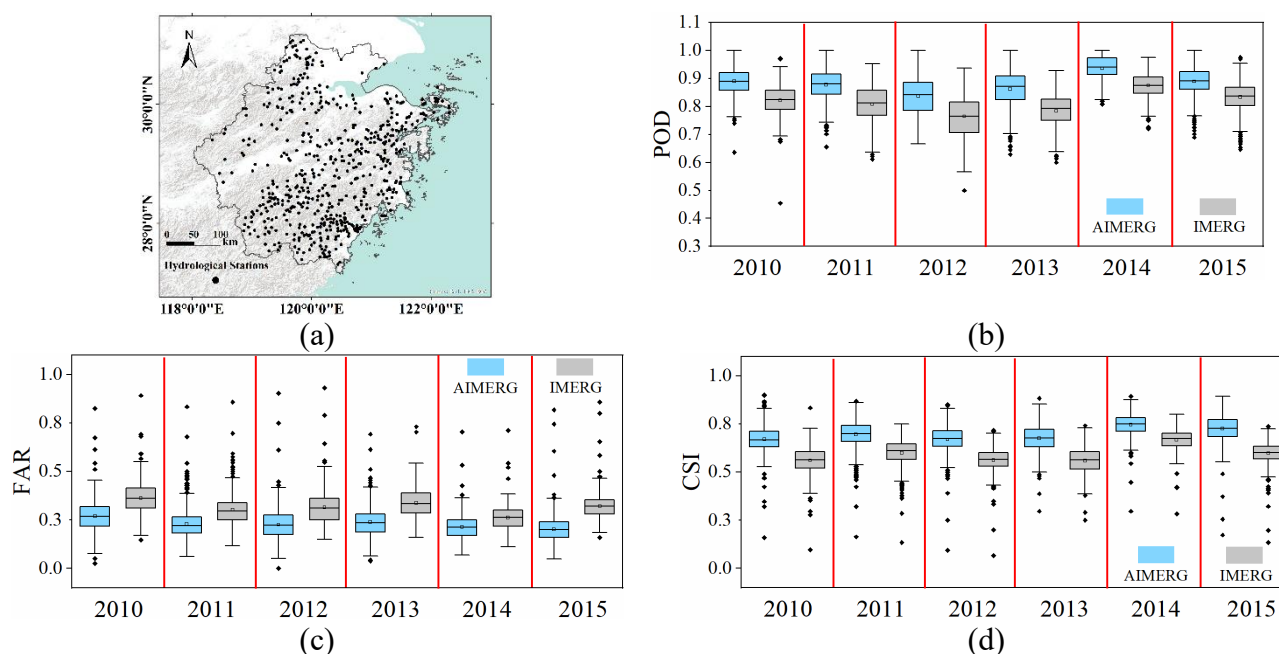
329 Figure 8. The boxplots demonstrated diagnose of IMERG and AIMERG against the ground observations
330 from the meteorological stations, at hourly scale, in six sub-regions, 2015.

331

332 To assess the quality of the IMERG and AIMERG, entirely independent precipitation data from
333 around 500 hydrological stations, at hourly scale, from 2010 to 2015, were applied, which were relatively
334 even distributed in Zhejiang province (Fig. 9a). The POD values of AIMERG (~ 0.9) were general larger
335 than those of IMERG (~ 0.8), while the FAR values of AIMERG (~ 0.3) were significantly smaller than
336 those of IMERG (~ 0.4), which resulted in the overall capabilities of AIMERG to capture the precipitation
337 events were improved more than 10%, compared with IMERG, in terms of the CSI. The relative smaller
338 POD values and larger FAR values of IMERG in the Zhejiang province, southeastern coast of China,



339 might be one of the potential drawbacks in accurately estimating the precipitation both qualitatively and
340 quantitatively.

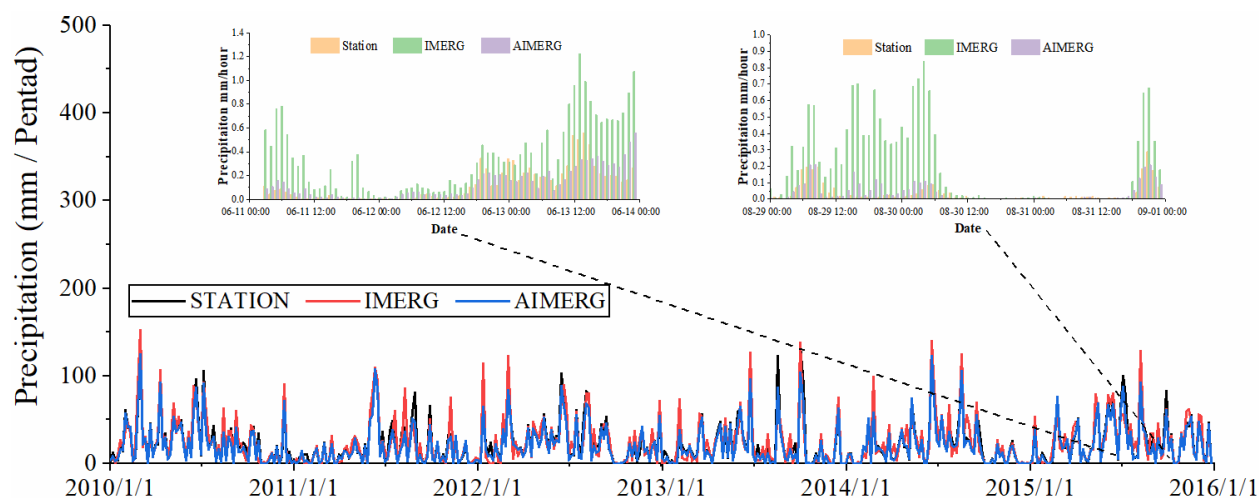


341 Figure 9. The boxplots demonstrated diagnose of IMERG and AIMERG against the ground observations
342 from hydrological stations, respectively, at hourly scale, in Zhejiang province, 2010-2015. The
343 background map used in this study was provided by Esri, USGS and NOAA
344 (http://goto.arcgisonline.com/maps/World_Terrain_Base, last access: 17 January 2020).

345 From the temporal patterns of mean areal precipitation of IMERG, AIMERG, and ground
346 observations from hydrological stations, in Zhejiang province, 2010-2015 (Fig. 10), IMERG were general
347 larger than both AIMERG and ground observations. For instance, the IMERG significantly overestimated
348 the precipitation with up to ten times than those of AIMERG and ground observations, such as in the



349 typical periods, 0 a.m., June, 11 – 0 a.m., June, 14, 2015, and 0 a.m., Aug, 29 – 0 a.m., Sep, 1, 2015.
350 Additionally, both the temporal patterns and the magnitudes of AIMERG were almost same with those
351 of ground observations, compared with those of IMERG. Meanwhile, in some pentads with the heavy
352 rain events, both AIMERG and ground observations were larger than IMERG.



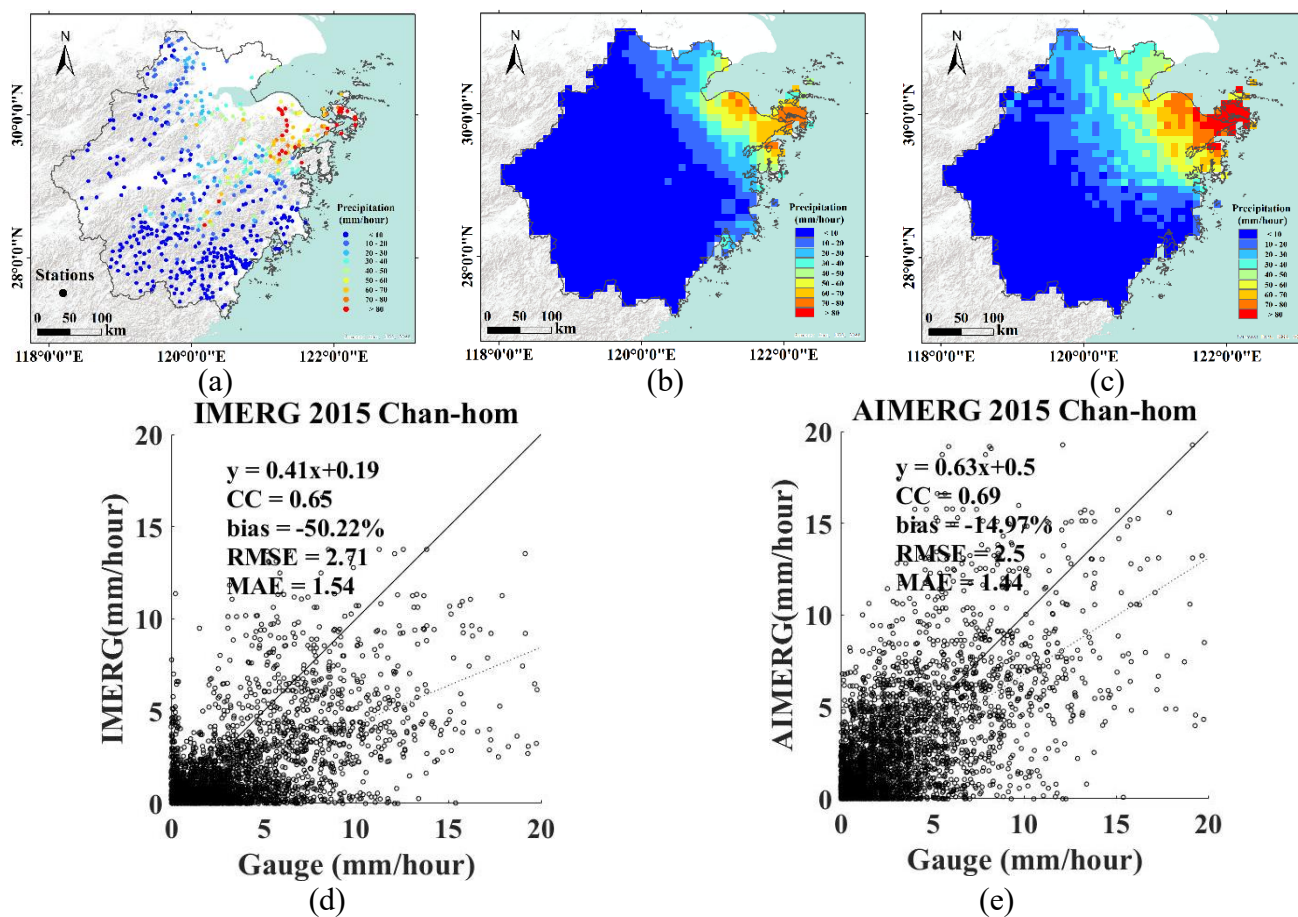
353
354 Figure 10. The temporal patterns of mean areal precipitation of IMERG, AIMERG, and the ground
355 observations from the independent hydrological stations, at daily/hourly scale, in Zhejiang province,
356 2010-2015.

357
358 One of the primary aims of the satellite-based precipitation estimates is to provide the high quality
359 precipitation information at hourly scale in the heavy rainfall events. Therefore, one typhoon event, Chan-
360 hom, was selected as an example for assessing the quality of the IMERG and AIMER in Zhejiang



361 Province, where is always threatened by the typhoons, shown in Fig. 11. Though the spatial patterns of
362 IMERG and AIMERG were both similar to those of ground observations, IMERG still underestimated
363 the precipitation, compared with AIMERG (Fig. 11 a-c). From the statistics, not only the systematic bias
364 of IMERG (around -50%) was significantly improved, with bias of AIMERG around -10%, but also the
365 random errors of IMERG (RMSE ~ 2.7 mm/hour, MAE ~ 1.5 mm/hour) were also reduced, compared
366 with AIMERG (RMSE ~ 2.5 mm/hour, MAE ~ 1.4 mm/hour), which meant the calibrations using
367 APHRODITE on IMERG improved the abilities of original IMERG product to more accurately estimate
368 the quantitative precipitation volumes, especially in heavy rainfall events (Fig. 11 c-d).

369



370 Figure 11. The typhoon, Chan-hom, was selected as an example for assessing the quality of the IMERG
371 and AIMER, occurred in the typical period 0 a.m., – 11 a.m., June, 11, 2015, in Zhejiang Province. The
372 background map used in this study was provided by Esri, USGS and NOAA
373 (http://goto.arcgisonline.com/maps/World_Terrain_Base, last access: 17 January 2020).

374

375 5. Discussions

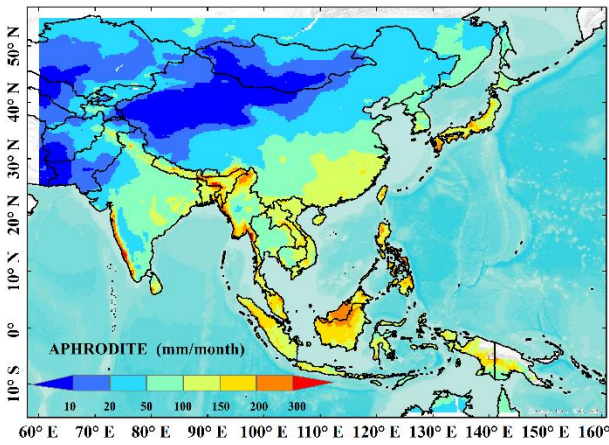


376 **5.1. The potential drawbacks in processing the IMERG product**

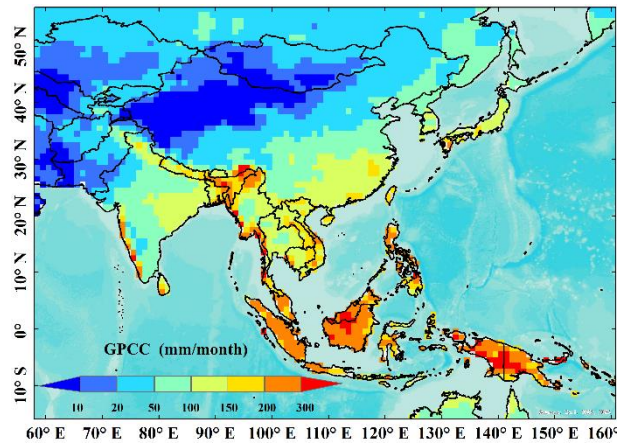
377 From the document of “Algorithm Theoretical Basis Document (ATBD) Version 06” for
378 generating the Final IMERG product (Huffman et al., 2019), we found that there were mainly two steps
379 in the process: the first step was to derive the satellite-based only precipitation inversion estimates, and
380 the second step was to calibrate the satellite-based only precipitation estimates using the interpolated
381 precipitation product based on ground observations, e.g., GPCC (monthly, $1.0^{\circ} \times 1.0^{\circ}$). As there is no
382 mature calibration algorithm for calibrating the satellite-based only precipitation estimates at daily scale,
383 the current IMERG-Final product are only calibrated using the GPCC at monthly scale. The two aims of
384 this study were to (1) provide a spatio-temporal calibration algorithm (DSTDCA) for anchoring the
385 satellite-based precipitation estimates at daily scale, and (2) a new precipitation product with finer quality,
386 namely AIMERG (half-hourly, $0.1^{\circ} \times 0.1^{\circ}$, 2000-2015, Asia) (Ma et al., 2020a, b), for Asian researcher.
387 For anchoring the IMERG final product, we introduced the APHRODITE data (daily, $0.25^{\circ} \times 0.25^{\circ}$,
388 2000-2015, Asia), which were interpolated based on ground observations from the large numbers of rain
389 gauges. Though the general spatial patterns of monthly mean precipitation estimates from both
390 APHRODITE and GPCC, from 1951 to 2015, were similar, the volumes of them demonstrated significant
391 differences, especially along the Himalayas, coastal Indochina and Western Ghats, and the Indonesia (Fig.
392 12 a-b). To much more clearly demonstrate the relative values of GPCC and APHRODITE, the spatial
393 patterns of the ratio of monthly mean values of APHRODITE to those of GPCC were illustrated in Fig.



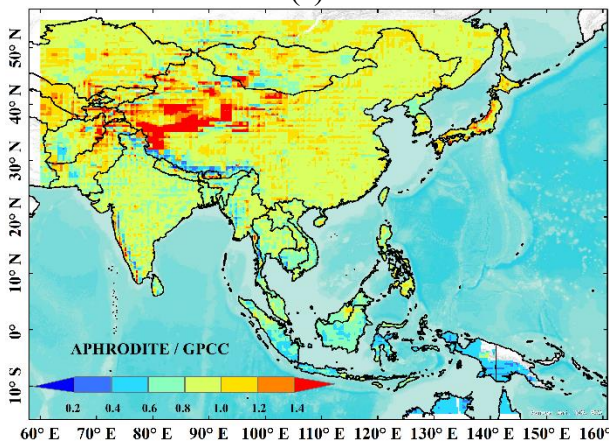
394 12 c, from which we found that GPCC significantly overestimated the precipitation in the tropical rain
395 range along the Indonesia, and along the southern Himalayas with complex terrain, while it significantly
396 underestimated the precipitation in the north western Tibetan Plateau and Middle East, compared with
397 the ground “truth” product, APHRODITE. Illustrated by Fig. 12, the GPCC plays vital roles for the final
398 IMERG product, and the introduction of APHRODITE on calibrating the IMERG would be greatly
399 benefiting the quality of the AIMERG.



(a)



(b)





(c)

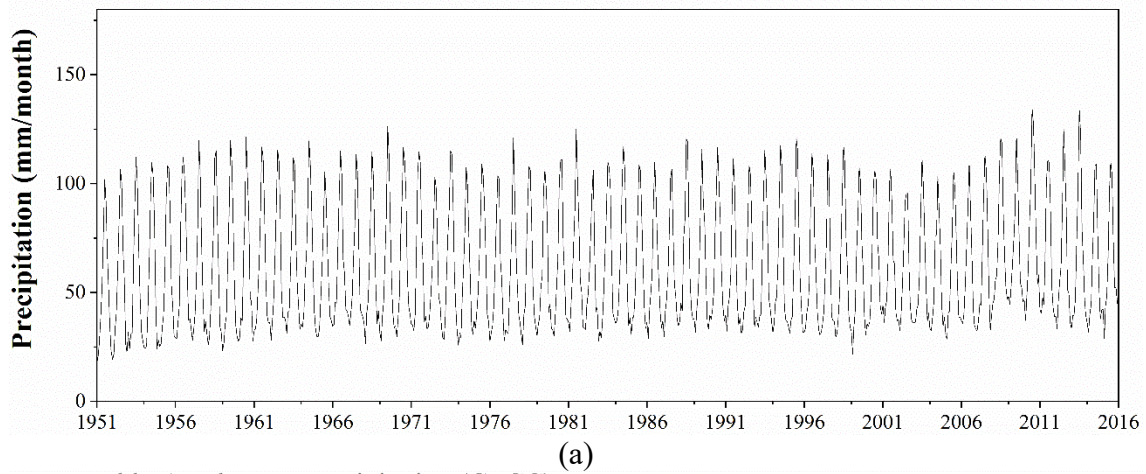
400 Figure 12. The spatial patterns of the monthly mean precipitation of (a) APHRODITE and (b) GPCC, and
401 (c) Ratio between monthly mean values of APHRODITE and GPCC, over the Asia in the period from
402 1951 to 2015. The background map used in this study was provided by Esri, USGS and NOAA
403 (http://goto.arcgisonline.com/maps/World_Terrain_Base, last access: 17 January 2020).

404 There were mainly two kinds of errors in the satellite-based precipitation product, including
405 systematic bias and random errors (Shen et al., 2014). As seen in the above-mentioned results, the random
406 errors of the AIMERG were alleviated by using the APHRODITE data compared with IMERG (e.g., Fig.
407 4-11). In terms of the systematic errors, we compared the monthly Asian mean precipitation estimates of
408 both APHRODITE and GPCC, from 1951 to 2015 (Fig. 13). The monthly Asian mean precipitation of
409 APHRODITE varied between ~ 25 mm/month and ~ 100 mm/month, while those of GPCC ranged from
410 ~ 50 mm/month and ~ 150 mm/month, which resulted the ratios of APHRODITE to GPCC fluctuated
411 significantly from ~ 0.2 to ~ 0.9, with average value ~ 0.7, which meant that the GPCC at least
412 overestimated the precipitation more than ~ 30%, compared with the APHRODITE. Therefore, the
413 introduction of APHRODITE data would greatly reduce the systematic errors of the IMERG final product,
414 over the Asia.

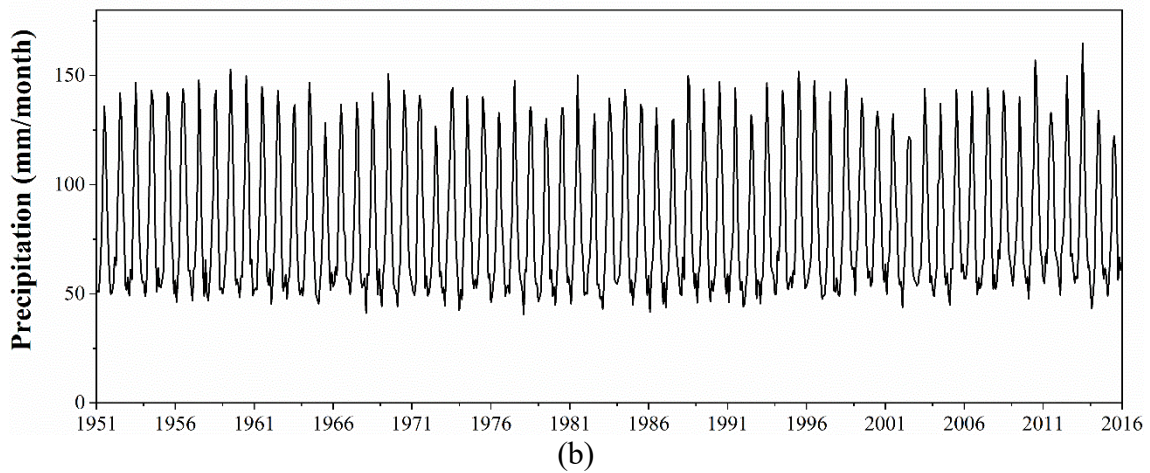
415

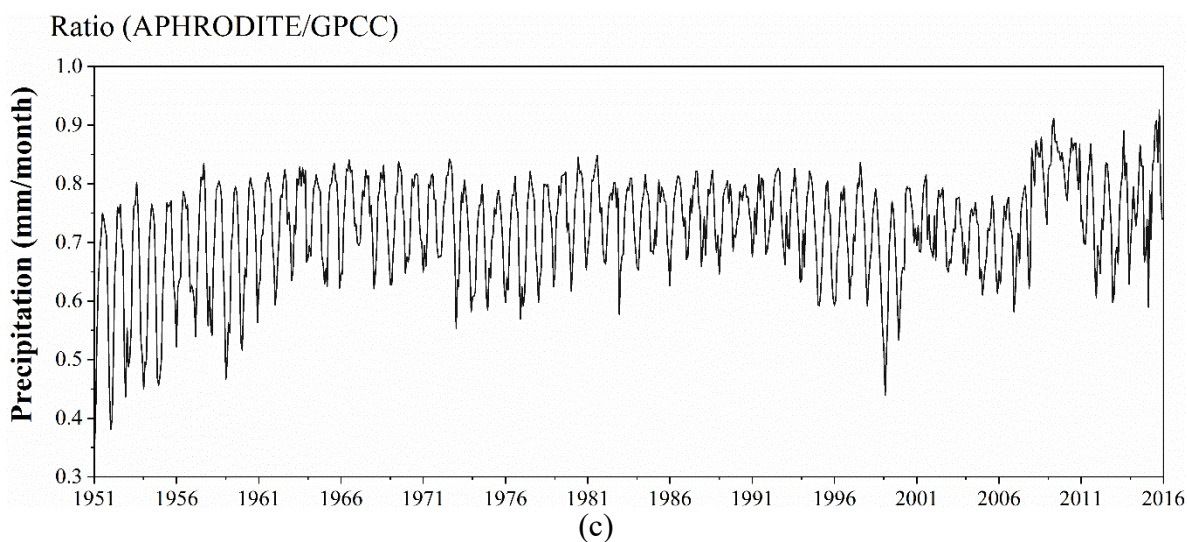


Monthly Areal Mean Precipitation (APHRODITE)



Monthly Areal Mean Precipitation (GPCC)





416 Figure 13. The temporal patterns of monthly areal mean precipitation of (a) APHRODITE, (b) GPCC,
417 and (c) APHRODITE/GPCC, 1951-2015.

418 5.2. The controls on the range of the spatial weights based on IMERG

419 As demonstrated in the document of the “ATBD”, gauge information is introduced into the original
420 multi-satellite-only half-hourly data to generate the final IMERG product. Firstly, the ratio between the
421 monthly accumulation of half-hourly multi-satellite-only field and the monthly satellite-gauge field is
422 calculated, then each half-hourly field of multi-satellite-only precipitation estimates in the corresponding
423 month is multiplied by the ratio field to generate the half-hourly calibrated IMERG. After various
424 experiments, the ratio values between the monthly satellite-gauge and the monthly accumulation of half-
425 hourly multi-satellite-only fields is limited to the range [0.2, 3] (Huffman et al., 2019). The cap of 3 was
426 decided due to the value of 2 (used in TRMM V6) was too restrictive. Additionally, the cap of 3 was



427 finally applied because it performed better in matching the two accumulations than that of other larger
428 values, for instance, the cap of 4 resulted in introducing unrealistic shifts to histogram of half-hourly
429 precipitation rates for the month. Additionally, early in TRMM the lower bound of 0.5 was applied, which
430 suggests a smaller value of the lower bound allows matching between the two accumulations without
431 creating the egregious high snapshot values when the upper bound is expanded too far.

432 Inspired by the range of the ratio values between the monthly satellite-gauge and the monthly
433 accumulation of half-hourly multi-satellite-only fields in generating IMERG, we considered the range [0,
434 1.5] of the daily spatial disaggregation weights in this study was reasonable after careful checking the
435 distributions of spatial disaggregation weights. The lower bound of 0 was selected based on the
436 consideration if the IMERG did not capture the daily precipitation event, then the spatial disaggregation
437 weight is still equal to zero, which agreed as most as possible to the original IMERG. While there were
438 at least two reasons for setting the upper bound of the spatial disaggregation weights as 1.5: (1) most
439 numerical values of spatial disaggregation weights were in the range [0, 1.5], and (2) there were obvious
440 anomalies in the final calibrated AIMERG, especially along the coastal regions and edges of the specific
441 precipitation event coverages, where the values of the spatial disaggregation weights were larger than 1.5.
442 Though the range [0, 1.5] of spatial disaggregation weights was applied to obtain the final AIMERG in
443 this study, we also considered that this was still an open-ended question.

444 **5.3. The advantages of APHRODITE data in anchoring the satellite-based precipitation product**



445 It has been a great challenge to obtain precipitation estimates over the Tibetan Plateau and its
446 surroundings, as there were very limited ground observations in this region, especially in its western parts
447 (Ma et al., 2017). Incorporating a uniform precipitation gauge analysis is important and critical for
448 controlling the bias that typifies the satellite precipitation estimates, e.g., using GPCC for TMPA and
449 IMERG (Huffman et al., 2019). Those projects (e.g., GPCC, TRMM, GPM) demonstrated that even
450 monthly gauge analyses contributed significant improvements on the satellite-only precipitation estimates,
451 at least for some regions in some seasons. Primarily explorations at CPC suggested substantial
452 improvements in the bias corrections using daily gauge analysis, especially for regions, where there is a
453 dense network of gauges. Foreseeably, GPM would try their best to calibrate the GPM satellite-only
454 precipitation estimates at finer spatio-temporal scales (e.g., 0.25°/daily) worldwide.

455 Currently, GPCC were used to calibrate the TRMM TMPA and GPM IMERG at monthly scale. The
456 Deutscher Wetterdienst (DWD) Global Precipitation Climatology Centre (GPCC) was established in
457 1989 to provide high-quality precipitation analyses over land based on conventional precipitation gauges
458 from ~7,000-8,000 stations world-wide (Schneider et al. 2014, 2018). And two GPCC products were
459 applied in the IMERG, the V8 Full Data Analysis for the majority of the time (currently 1998-2016), and
460 the V6 Monitoring Product from 2017 to the then-present. Compared with GPCC, APHRODITE has
461 inherently advantages with significantly larger numbers of ground observations and finer spatio-temporal
462 resolutions, over the Asia. APHRODITE projects aimed at collecting as most gauge information as
463 possible from the Asian countries. There were mainly three kinds of gauge information sources used in



464 APHRODITE analysis, the GTS-based data, data precompiled by other projects or organizations, and
465 APHRODITE's own collection. More detailed information on the APHRODITE' data sources could be
466 found at the website (<http://www.chikyu.ac.jp/precip/>) and the research of Yatagai (2012). Compared
467 with the GPCC with the limited ground observations in and around the Tibetan Plateau in China, the
468 neighboring countries provided plenty of ground observations in the APHRODITE data, in mountainous
469 regions, and semi-arid and arid regions. Additionally, the spatio-temporal resolutions of APHRODITE
470 (0.25° /daily) were finer than those of GPCC (1.0° /monthly). Therefore, APHRODITE has significant
471 advantages in calibrating the IMERG data at daily scale.

472 The extent of the AIMERG could cover the Northern Eurasia, Middle East, Monsoon Asia, and
473 Japan. This study mainly evaluated the AIMERG in the China Mainland, which calls for Asia wide
474 evaluations in the future to assess both the algorithm and the corresponding precipitation product.

475 **6. Data Availability**

476 The AIMERG data record (0.1° /half-hourly, 2000-2015, Asia) is freely available at [http://argi-](http://argi-basic.hihanlin.com:8000/d/d925fecf60/)
477 [basic.hihanlin.com:8000/d/d925fecf60/](http://argi-basic.hihanlin.com:8000/d/d925fecf60/). Additionally, the AIMERG data is also freely accessible at
478 <https://doi.org/10.5281/zenodo.3609352> (for the period from 2000 to 2008) (Ma et al., 2020a) and
479 <https://doi.org/10.5281/zenodo.3609507> (for the period from 2009 to 2015) (Ma et al., 2020b).

480 .



481

482 **7. Conclusions**

483 As the milestone in the satellite-based precipitation measurement process, the TRMM and its
484 successor GPM generate the most popular and the state-of-the-art satellite precipitation products for both
485 water cycle related scientific research and applications, TMPA (1998-present, 0.25°/3 hourly) and
486 IMERG (2014-present, 0.1°/half-hourly), as well as the retrospective IMERG (2000-present, 0.1°/half-
487 hourly) from GPM era to TRMM era. In this study, focusing on the potential drawbacks in generating
488 IMERG and its recently updated retrospective IMERG (finished in July, 2019), which were only
489 calibrated at monthly scale using limited ground observations, GPCC (1.0°/monthly), resulting the
490 IMERG with large systematic bias and random errors, we introduced another daily gauge analysis product,
491 APHRODITE (Last update October 5, 2018), to calibrate the IMERG at 0.25°/daily scale. Compared with
492 GPCC, APHRODITE has inherently advantages with significantly larger numbers of ground observations
493 and finer spatio-temporal resolutions (0.25°/daily), over the Asia.

494 We have proposed a new algorithm (Daily Spatio-Temporal Disaggregation Calibration Algorithm,
495 DSTDCA) for calibrating IMERG at daily scale, and provided a new AIMERG precipitation dataset
496 (0.1°/half-hourly, 2000-2015, Asia) (Ma et al., 2020a, b) with better quality, calibrated by APHRODITE
497 at daily scale for the Asian applications. And the main conclusions included but not limited to: (1) the
498 proposed daily calibration algorithm was effective in considering the advantages from both satellite-



499 based precipitation estimates and the ground observations; (2) AIMERG performed better than IMERG
500 at different spatio-temporal scales, in terms of both systematic biases and random errors, over the China
501 Main land; and (3) APHRODITE demonstrated significant advantages than GPCP in calibrating the
502 IMERG, especially over the mountainous regions with complex terrain, e.g., the Tibetan Plateau.
503 Additionally, Results of this study suggests that it is a promising and applicable daily calibration
504 algorithm for GPM in generating the future IMERG in either operational scheme or retrospective manner.

505

506 **Author Contributions**

507 Dr. Ziqiang Ma designed and organized the manuscript. Drs. Jintao Xu, Siyu Zhu, and Yuanjian
508 Yang prepared the related materials and run the models for generating AIMERG and the related
509 assessments. Dr. Guoqiang Tang and Prof. Zhou Shi made contributions on the scientific framework of
510 this study and discussed the interpretation of results. Prof. Yang Hong co-advised this study. All authors
511 discussed the results and commented on the manuscript.

512

513 **Competing interests**

514 The authors declare they have no competing financial interests.

515



516 **Acknowledgments**

517 This study was financially supported by the National Natural Science Foundation of China (Grant
518 No. 41901343); the Key R&D Program of Ministry of Science and Technology, China (Grant No.
519 2018YFC1506500); the China Postdoctoral Science Foundation (No. 2018M630037, and 2019T120021);
520 the Open Fund of the State Key Laboratory of Remote Sensing Science, China (Grant No.
521 OFSLRSS201909), the State Key Laboratory of Resources and Environmental Information System,
522 China.

523 The contribution of the data providers is also greatly appreciated, including the Chinese
524 Meteorological Data Sharing Service System (<http://cdc.nmic.cn/home.do>), the APHRODITE data
525 provider (<http://aphrodite.st.hirosaki-u.ac.jp/download/>), and the IMERG data provider
526 (<https://pmm.nasa.gov/data-access/downloads/gpm>).

527

528 **References**

529 Adler, R. F., Huffman, G. J., Chang, A., Ferraro, R., Xie, P., Janowiak, J., Rudolf, B., Schneider, U.,
530 Curtis, S., Bolvin, D., Gruber, A., Susskind, J., Arkin, P., and Nelkin, E.: The Version-2 Global
531 Precipitation Climatology Project (GPCP) Monthly Precipitation Analysis (1979–Present), J.



- 532 Hydrometeorol., 4, 1147–1167, <https://doi.org/10.1175/1525->
533 7541(2003)004<1147:TVGPCP>2.0.CO;2, 2003.
- 534 Beck, H. E., van Dijk, A. I. J. M., Levizzani, V., Schellekens, J., Miralles, D. G., Martens, B., and Roo,
535 A. d.: MSWEP: 3-hourly 0.25° global gridded precipitation (1979–2015) by merging gauge,
536 satellite, and reanalysis data, *Hydrol. Earth Syst. Sci.*, 21, 589–615, <https://doi.org/10.5194/hess-21->
537 589-2017, 2017.
- 538 Beck, H. E., Wood, E. F., Pan, M., Fisher, C. K., Miralles, D. G., van Dijk, A. I. J. M., McVicar, T. R.,
539 and Adler, R. F.: MSWEP V2 Global 3-Hourly 0.1° Precipitation: Methodology and Quantitative
540 Assessment, *Bull. Amer. Meteorol. Soc.*, 100, 473–500, <https://doi.org/10.1175/BAMS-D-17->
541 0138.1, 2018.
- 542 Chen, M., Xie, P., Janowiak, J., and Arkin, P.: Global Land Precipitation: A 50-yr Monthly Analysis
543 Based on Gauge Observations, *J. Hydrometeorol.*, 3, 249–266, <https://doi.org/10.1175/1525->
544 7541(2002)003<0249:GLPAYM>2.0.CO;2, 2002.
- 545 Duncan, J. M. A., and Biggs, E. M.: Assessing the accuracy and applied use of satellite-derived
546 precipitation estimates over Nepal, *Appl. Geogr.*, 34, 626–638,
547 <https://doi.org/10.1016/j.apgeog.2012.04.001>, 2014.



- 548 Ebert, E. E., Janowiak, J. E., and Kidd, C.: Comparison of Near-Real-Time Precipitation Estimates from
549 Satellite Observations and Numerical Models, *Bull. Amer. Meteorol. Soc.*, 88, 47-64,
550 <https://doi.org/10.1175/BAMS-88-1-47>, 2007.
- 551 Hamada, A., Arakawa, O., and Yatagai, A.: An automated quality control method for daily rain-gauge
552 data, *Global Environmental Research*, 15, 183-192, http://www.airies.or.jp/journal_15-2eng.html,
553 2011.
- 554 Hong, Y., Hsu, K.-L., Sorooshian, S., and Gao, X.: Precipitation Estimation from Remotely Sensed
555 Imagery Using an Artificial Neural Network Cloud Classification System, *J. Appl. Meteorol.*, 43,
556 1834-1853, <https://doi.org/10.1175/JAM2173.1>, 2004.
- 557 Huffman, G. J., Bolvin, D. T., Nelkin, E. J., Wolff, D. B., Adler, R. F., Gu, G., Hong, Y., Bowman, K. P.,
558 and Stocker, E. F.: The TRMM Multisatellite Precipitation Analysis (TMPA): Quasi-Global,
559 Multiyear, Combined-Sensor Precipitation Estimates at Fine Scales, *J. Hydrometeorol.*, 8, 38-55,
560 <https://doi.org/10.1175/JHM560.1>, 2007.
- 561 Huffman, G. J., Bolvin, D. T., Braithwaite, D., Hsu, K., Joyce, R., Kidd, C., Nelkin, E. J., and Xie, P.:
562 NASA Global Precipitation Measurement (GPM) Integrated Multi-satellite Retrievals for GPM
563 (IMERG), Algorithm Theoretical Basis Document (ATBD), NASA/GSFC, Greenbelt, MD, USA,
564 38pp., 2014.



- 565 Huffman, G. J., E.F. Stocker, D.T. Bolvin, E.J. Nelkin, and Jackson Tan: GPM IMERG Final
566 Precipitation L3 Half Hourly 0.1 degree x 0.1 degree V06, Greenbelt, MD, Goddard Earth Sciences
567 Data and Information Services Center (GES DISC), <https://doi.org/10.5067/GPM/IMERG/3B->
568 HH/06, 2019.
- 569 Joyce, R. J., Janowiak, J. E., Arkin, P. A., and Xie, P.: CMORPH: A Method that Produces Global
570 Precipitation Estimates from Passive Microwave and Infrared Data at High Spatial and Temporal
571 Resolution, *J. Hydrometeorol.*, 5, 487-503, <https://doi.org/10.1175/1525->
572 7541(2004)005<0487:CAMTPG>2.0.CO;2, 2004.
- 573 Lu, H., Ding, L., Ma, Z., Li, H., Lu, T., Su, M., and Xu, J.: Spatiotemporal Assessments on the Satellite-
574 Based Precipitation Products From Fengyun and GPM Over the Yunnan-Kweichow Plateau, China,
575 *Earth Space Sci.*, 7, e2019EA000857, <https://doi.org/10.1029/2019EA000857>, 2020.
- 576 Ma, Z., Jin, X., Zhu, S., Tang, G., Yang, Y., Shi, Z., and Hong, Y.: AIMERG: a new Asian precipitation
577 dataset (0.1°/half-hourly, 2000-2008) by calibrating GPM IMERG at daily scale using
578 APHRODITE [Data set], Zenodo, <https://doi.org/10.5281/zenodo.3609352>, 2020.
- 579 Ma, Z., Jin, X., Zhu, S., Tang, G., Yang, Y., Shi, Z., and Hong, Y.: AIMERG: a new Asian precipitation
580 dataset (0.1°/half-hourly, 2009-2015) by calibrating GPM IMERG at daily scale using
581 APHRODITE [Data set], Zenodo, <https://doi.org/10.5281/zenodo.3609507>, 2020.
- 582 Ma, Z., Shi, Z., Zhou, Y., Xu, J., Yu, W., and Yang, Y.: A spatial data mining algorithm for downscaling



- 583 TMPA 3B43 V7 data over the Qinghai–Tibet Plateau with the effects of systematic anomalies
584 removed, *Remote Sens. Environ.*, 200, 378-395, <https://doi.org/10.1016/j.rse.2017.08.023>, 2017.
- 585 Matsuura, K., and Willmott C. J.: Terrestrial precipitation: 1900–2008 gridded monthly time series
586 (version 2.01), Center for Climatic Research Department of Geography Center for Climatic
587 Research, University of Delaware,
588 http://climate.geog.udel.edu/~climate/html_pages/Global2_Ts_2009/README_global_p_ts_2009.html, 2009.
- 590 Mitchell, T. D., and Jones, P. D.: An improved method of constructing a database of monthly climate
591 observations and associated high-resolution grids, *Int. J. Climatol.*, 25, 693-712,
592 <https://doi.org/10.1002/joc.1181>, 2005.
- 593 Rajeevan, M., and Bhate, J.: A high resolution daily gridded rainfall dataset (1971–2005) for mesoscale
594 meteorological studies, *Curr. Sci.*, 96, 558-562, <https://www.jstor.org/stable/24105470>, 2009.
- 595 Schneider, U., Fuchs, T., Meyer-Christoffer, A., and Rudolf, B.: Global precipitation analysis
596 products of the GPCC. Global Precipitation Climatology Centre, DWD, 13 pp., 2008
- 597 Schneider, U., Becker, A., Finger, P., Meyer-Christoffer, A., Ziese, M., and Rudolf, B.: GPCC's new land
598 surface precipitation climatology based on quality-controlled in situ data and its role in
599 quantifying the global water cycle, *Theor. Appl. Climatol.*, 115, 15-40,
600 <https://doi.org/10.1007/s00704-013-0860-x>, 2014.
- 601 Schneider, U., P. Finger, A. Meyer-Christoffer, M. Ziese, A. Becker: Global Precipitation Analysis



- 602 Products of the GPCC. GPCC Internet Publication, DWD, 17 pp., 2018
- 603 Shen, Y., Feng, M. N. Zhang, H. Z. and Gao, X.: Interpolation methods of China daily precipitation data
604 [in Chinese], *J. Appl. Meteorol. Sci.*, 21, 279–286, <https://doi.org/10.11898/1001-7313.20100303>,
605 2010.
- 606 Shen, Y., Zhao, P., Pan, Y., and Yu, J.: A high spatiotemporal gauge-satellite merged precipitation analysis
607 over China, *J. Geophys. Res. Atmos.*, 119, <https://doi.org/10.1002/2013JD020686>, 2014.
- 608 Sorooshian, S., Hsu, K.-L., Gao, X., Gupta, H. V., Imam, B., and Braithwaite, D.: Evaluation of
609 PERSIANN System Satellite-Based Estimates of Tropical Rainfall, *Bull. Amer. Meteorol. Soc.*,
610 81, 2035-2046, [https://doi.org/10.1175/1520-0477\(2000\)081<2035:EOPSSE>2.3.CO;2](https://doi.org/10.1175/1520-0477(2000)081<2035:EOPSSE>2.3.CO;2), 2000.
- 611 Tang, G., Ma, Y., Long, D., Zhong, L., and Hong, Y.: Evaluation of GPM Day-1 IMERG and TMPA
612 Version-7 legacy products over Mainland China at multiple spatiotemporal scales, *J. Hydrol.*, 533,
613 152-167, <https://doi.org/10.1016/j.jhydrol.2015.12.008>, 2016.
- 614 Xie, P., and Xiong, A.-Y.: A conceptual model for constructing high-resolution gauge-satellite merged
615 precipitation analyses, *J. Geophys. Res. Atmos.*, 116, <https://doi.org/10.1029/2011JD016118>,
616 2011.
- 617 Xu, J., Ma, Z., Tang, G., Ji, Q., Min, X., Wan, W., and Shi, Z.: Quantitative Evaluations and Error Source
618 Analysis of Fengyun-2-Based and GPM-Based Precipitation Products over Mainland China in
619 Summer, 2018, *Remote Sens.*, 11, <https://doi.org/10.3390/rs11242992>, 2019.



620 Yatagai, A., Xie, P., and Kitoh, A.: Utilization of a New Gauge-based Daily Precipitation Dataset over
621 Monsoon Asia for Validation of the Daily Precipitation Climatology Simulated by the MRI/JMA
622 20-km-mesh AGCM, SOLA, 1, 193-196, <https://doi.org/10.2151/sola.2005-050>, 2005.

623 Yatagai, A., Kamiguchi, K., Arakawa, O., Hamada, A., Yasutomi, N., and Kitoh, A.: APHRODITE:
624 Constructing a Long-Term Daily Gridded Precipitation Dataset for Asia Based on a Dense Network
625 of Rain Gauges, Bull. Amer. Meteorol. Soc., 93, 1401-1415, [https://doi.org/10.1175/BAMS-D-11-](https://doi.org/10.1175/BAMS-D-11-00122.1)
626 00122.1, 2012.

627 Yong, B., Ren, L.-L., Hong, Y., Wang, J.-H., Gourley, J. J., Jiang, S.-H., Chen, X., and Wang, W.:
628 Hydrologic evaluation of Multisatellite Precipitation Analysis standard precipitation products in
629 basins beyond its inclined latitude band: A case study in Laohahe basin, China, Water Resour. Res.,
630 46, <https://doi.org/10.1029/2009WR008965>, 2010.

631

632

633



634 **Appendix A: Acronyms with definitions used in this study.**

AIMERG	Asian precipitation dataset by calibrating GPM IMERG at daily scale using
APHRODITE	
APHRODITE	Asian Precipitation Highly Resolved Observational Data Integration Towards Evaluation of Water Resources
ATBD	Algorithm Theoretical Basis Document
BIAS	Relative Bias
CC	Correlation Coefficient
CLIMAT	Monthly Climatological Data
CMA	Chinese Meteorological Administration
CMORPH	CPC Morphing
CPC	Climate Prediction Center
CSI	Critical Success Index
DSTDCA	Daily Spatio-Temporal Disaggregation Calibration Algorithm
DWD	Deutscher Wetterdienst
FAR	False Alarm Ratio
GEWEX	Global Energy and Water Exchange
GPCC	Global Precipitation Climatology Centre
GPM	Global Precipitation Measurement
GTS	Global Telecommunications System



IDW	Inverse Distance Weighting
IMERG	Integrated Multi-satellitE Retrievals for GPM
IR	Infrared
ME	Mean Error
MW	Microwave
NHMs	National hydrological and meteorological services
NMIC	National Meteorological Information Center
PERSIANN	Precipitation Estimation from Remotely Sensed Information using Artificial Neural Networks
PERSIANN-	Precipitation Estimation from Remotely Sensed Information using Artificial Neural
CCS	Networks-Cloud Classification System
PMW	Passive Microwave
POD	Probability of Detection
QC	Quality Control
RMSD	Root-mean-square Deviation
RMSE	Root Mean Square Error
SG	Satellite-Gauge
SYNOP	Synoptic Weather Report
TMPA	TRMM Multi-satellite Precipitation Analysis
TRMM	Tropical Rainfall Measuring Mission